Efficient removal of Cr (VI) and Co (II) from aqueous solution by activated carbon from *Manihot esculenta* Crantz agricultural bio-waste

A. Belcaid, B. H. Beakou, K. El Hassani, S. Bouhsina and A. Anouar

ABSTRACT

Heavy metals are one of the most dangerous and critical threats to human and environment. In this study, the adsorption efficiency of activated carbon from cassava peels considered as agricultural waste (CPR) was evaluated for removal of heavy metals Cr (VI) and Co (II) from aqueous media. Cassava peel carbon (CPC) was obtained by acid treatment. Structural and morphological properties were investigated using Fourier Transform Infra-Red (FTIR), Scanning Electron Microscopy (SEM), Brunauer-Emmet-Teller surface area (BET) and X-Ray Diffraction (XRD). The adsorption experiments were conducted in batch mode under natural solution pH and complexation of the heavy metals, which allows the use of UV-Visible spectroscopy technique. CPC adsorbent exhibited a high adsorption capacity, according to Langmuir model, for Cr (VI) (166.35 mg/g) and Co (II) (301.63 mg/g) at 25 °C. Kinetic and adsorption isotherms followed the pseudo second-order and Langmuir isotherm models for both metals, respectively. Thermodynamic study confirmed the spontaneity and endothermic nature of both metals adsorption onto CPC surface.

Key words | activated carbon, adsorption, cassava peel, chromium, cobalt

A. Belcaid
B. H. Beakou
K. El Hassani (corresponding author)
A. Anouar
Faculty of Science and Technology, Laboratory of Applied Chemistry and Environment,
Hassan First University of Settat,
Settat, 26000
Morocco
E-mail: *k.elhassani@uhp.ac.ma*

S. Bouhsina
Unit of Environmental Chemistry and Interactions with Life,
University Littoral Côte d'Opale,
Dunkirk, 59140
France

HIGHLIGHTS

- Cassava peel carbon (CPC) was obtained by low-temperature pyrolysis at 350 °C.
- Cr(VI) and Co(II) adsorption was performed in a batch mode.
- CPC showed high efficiency in Cr(VI) and Co(II) removal at natural solution pH.
- Spontaneous adsorption for both metals occurred at higher temperatures.

INTRODUCTION

The exponential expansion of industrial activities, caused by high growth of the population and urbanization, has increased industrial wastes and the discharge of a high percentage of toxic heavy metals such as cadmium, mercury, lead, copper, zinc, nickel, chromium and cobalt into the environment, perturbing the environment and posing serious health hazards to humans (Rai *et al.* 2019). The existence of heavy metals in our aquatic system may be instigated by aqueous solutions of many industries, such as automobile, mining, electroplating, iron–steel and battery industries (Akpomie & Dawodu 2015). Among the heavy metals, cobalt and chromium got more attention due to their dangerous effects. In fact, chromium has many oxidation states and Cr (VI) is the most harmful; its exposure limit is 0.05 mg/L according to the World Health Organization (WHO) (World Health Organization 2003). Chromium can cause cancer in the digestive tract and lungs, epigastric pain, nausea, severe diarrhea, vomiting and haemorrhage (Rangabhashiyam *et al.* 2016). Cobalt has an occupational exposure limit of 1 µg/L according to WHO (Office of Occupational Health 1996); above this

doi: 10.2166/wst.2020.585

limit it becomes harmful and toxic, inducing breathing problems, such as asthma and pneumonia. A high concentration of cobalt is responsible for vomiting, nausea, vision problems, heart problems and thyroid damage (Farjana *et al.* 2019).

Hence, various methods and treatment technologies that have been developed for the removal of heavy metals from aqueous solution include precipitation and sludge separation, chemical treatment, oxidation-reduction, ion exchange, reverse osmosis, coagulation, flocculation, electrochemical treatment, membrane processes, evaporation, and adsorption onto activated carbon (Javanbakht *et al.* 2014). However, these methods have disadvantages, like production of a large quantity of hazardous wastes (Saha *et al.* 2019), high costs in terms of energy consumption, low performance when heavy metals concentration is below 100 mg/L (Pugazhenthiran *et al.* 2016). Therefore, there is a necessity to find an effective process to remove heavy metals economically with less cost. Agricultural waste materials were used as activated carbon sources by different researchers. They represent unused resources and also, they are widely available with a great potential to be used as adsorbents (Hashemian *et al.* 2014).

Cassava (*Manihot esculenta* Crantz) is a crop largely cultivated in tropical and sub-tropical climates like in Africa (Benin, Nigeria), also in Asia (Indonesia, Thailand) and Latin America (Brazil). Taxonomically it belongs to the Euphorbiaceae family and Manihot genus. Cassava peel is an ideal renewable carbon source and millions of tons of this waste are generated every day (Salgaonkar *et al.* 2019). Cassava peels are used in many fields like the production of bio-ethanol, compost, also the generation of biofuel, chemicals, and finally in aqueous solution treatment as adsorbent for dyes (Beakou *et al.* 2017) and heavy metals (Tovar *et al.* 2019). Nevertheless, to well valorize cassava peel, there is still a need to investigate more the adsorption process to reach the highest metal removal rate. The aim of this work is to display the great potential of cassava peel used as precursor for activated carbon with proper activation. The work includes equilibrium, kinetics and thermodynamic study of adsorption of chromium and cobalt onto cassava peel carbon.

METHODS

Carbon preparation

The biomass used in this study, cassava peel tuber bark, was completely washed with distilled water and exposed to the sun light until it was totally dry, then finely ground and stored in a tightly closed container and called Cassava Peel Raw (CPR). The CPR product was ground and sieved to a particle size ranging from 40 to 63 μm. The mixture of the raw material (10 g) and phosphoric acid (mass ratio 1:1) was carried out in a beaker containing 200 mL of solution and heated at 75 °C for 14 hours, and then dried at 100 °C for 24 hours. The obtained product was ground and charred at 350 °C for 2 hours using a furnace model Nabertherm L40/11 Bo Germany under non inert conditions. After cooling in the open air, the support was washed thoroughly with distilled water. The resulting filtrate, poor in phosphoric acid, was dried, ground and soaked in 200 mL of $NaHCO_3$ (1%) for 14 hours to remove the residual acid and washed with distilled water until neutral pH. Finally, the activated carbon, named Cassava Peel Carbon (CPC), was dried at 60 °C for 6 hours and sieved to sizes between 40 and 63 μm.

Characterization

Different analytical methods were carried out in order to determine the functional groups, pore distribution, surface morphology and main compositions of the sample. The chemical characterization of the functional groups of CPC was detected using a Fourier Transform Infrared (FTIR) spectrophotometer model Varian 800/Gladiatr (Scimitar Series, Australia/Pike Technologies, USA). Infrared absorbance data were obtained for wavenumbers in the range of 400–4,000 cm^{-1} using 50 scans collected at 4 cm^{-1} resolution. Surface area and pore volume calculations were analysed by the Brunauer-Emmett-Teller (BET) and the Barrett-Joyner Halenda (BJH) equations, respectively, with nitrogen adsorption on the activated carbon surface at a temperature of 77 K. The measurements were conducted on Quadrasorb Si (Quantachrome, Germany). All the samples were firstly degassed at 150 °C for 24 hours. X-ray diffraction (XRD) analysis was carried out to identify the crystal structure of CPC by using a powder diffractometer (Phaser D2 Diffractometer, Broker, USA), with a Cu $K_{\alpha 1}$ radiation ($\lambda = 1.54060$ Å) operated at 30 KV and 10 mA. The spectra were recorded with a 2θ angle ranging from 2° to 90°. The surface morphology of CPC was investigated by scanning electron microscopy (SEM) analysis on PHENOM XL (Phenom-World, Netherland), with an accelerating voltage of 10 kV. The composition of CPC was evaluated using Energy-Dispersive X-Ray (EDX) spectroscopy, while the composition of cassava rind carbon was determined by an elementary analyser.

Adsorption measurements

Heavy metals solutions under study were prepared by dissolving the desired quantity of cobalt and chromium, separately, in 1,000 mL volumetric flasks. These solutions were diluted to prepare standard solutions of required concentration. Batch equilibrium studies were conducted under magnetic stirring rate of 300 rpm. The supernatants were separated by centrifugation at 7,500 rpm for 2 minutes (Sigma Laborzentrifugen, Germany) and collected using disposable syringes, followed by the complexation of cobalt and chromium solutions. Indeed, for cobalt solution, the complexation was performed in a 25 mL volumetric flask by adding 2 mL of hydrochloric acid (HCl), 5 mL of ammonium thiocyanate and 12 mL of acetone. Concerning the chromium, the complexation was performed also in a 25 mL volumetric flask by adding to the chromium solution 3 mL of diphenylcarbazide. The contents of the two flasks were made up to 25 mL with distilled water. Then the concentrations of cobalt and chromium solutions were determined by using an UV–Visible spectrophotometer DR 6,000 with RFID technology (HACH LANGE, GERMANY) at maximum absorbance wavelengths of 620 and 540 nm, respectively. The adsorption efficiency η (%) and the amount of both heavy metals adsorbed at equilibrium Q_e (mg/g) at time t (min) Q_t (mg/g), were calculated according to the following equations:

$$\eta = \frac{(C_i - C_e)}{C_i} \times 100 \quad (1)$$

$$Q_e = \frac{(C_i - C_e)V}{W} \quad (2)$$

C_i, C_e are the concentrations of metal ions at initial phase and equilibrium (mg/L), respectively. V is the volume of the solution (L), W is the weight of adsorbent (g).

The pH of cobalt and chromium was not modified. The natural pH values of cobalt and chromium solutions were equal to 4.6 and 3.8, respectively. Adsorption kinetic of heavy metals was studied at initial concentration of 20 mg/L of cobalt and chromium ion solutions separately in 200 mL Erlenmeyer flasks, mixed with 0.02 g of activated carbon at a temperature of 25 °C, and a contact time ranging from 5 to 180 min (3 hours). The mixture of metal ion solution and the adsorbent was shaken at 300 rpm in a double-jacketed beaker. Adsorption isotherms were also performed, using various chromium and cobalt concentrations in the range of 10–40 mg/L, with adsorbent dose of 0.02 g. The latter mixture was agitated in a rotary shaker at 300 rpm, in which temperature was maintained at 25 °C with a thermostat (Jp Selecta Frigiderm, Spain) for 3 hours. The thermodynamic adsorption was evaluated at different temperatures of 15, 25, and 35 °C; while keeping other parameters fixed: (i) activated carbon dose of 0.02 g, (ii) solution concentration of 35 mg/L, and (iii) magnetically stirring the mixture at 300 rpm in a double-jacketed beaker for 3 hours.

The fitting of adsorption kinetics, adsorption isotherms and the thermodynamic adsorption were performed separately with OriginPro data analysis and graphing software version 2018.

Desorption experiments

To understand more the mechanism of cobalt and chromium adsorption onto CPC, desorption experiments were performed. After performing the equilibrium study with different initial heavy metal concentrations ranging from 10 to 25 mg/L, the activated carbon particles were collected by filtration and then dried at 60 °C for 2 hours. Then, 100 mL of NaOH, distilled water and HNO_3 solutions were used separately for the regeneration study.

RESULTS AND DISCUSSION

Characterization

The X-ray diffraction measurements were performed to evaluate the crystallographic structure of CPR and CPC. The spectra in Figure 1 show the XRD patterns for both

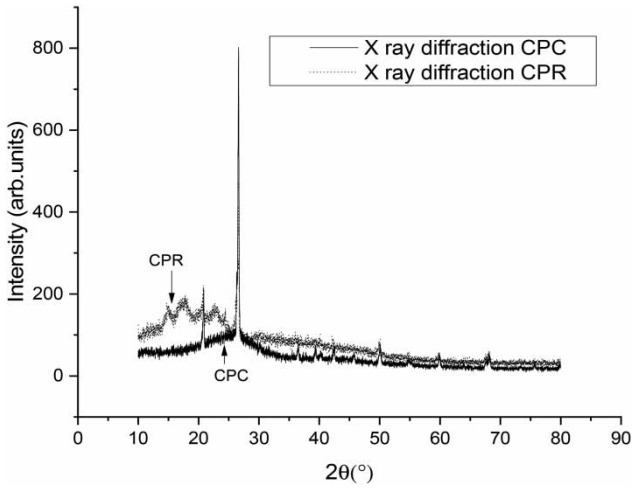

Figure 1 | X ray diffraction of cassava peel carbon and cassava peel raw.

materials. It is noted that the presence of very sharp diffraction peaks and the absence of broad peaks reveal an increasing regularity of crystalline structure and a better layer alignment for CPC, while CPR exhibited an amorphous structure with one sharp diffraction peak. Furthermore, the main diffraction peak was around $2\theta = 26°$, corresponding to the (002) plane, a characteristic peak of graphite (Zbair *et al.* 2018). The calcination temperature ($T = 350\,°C$) suggests the start of the graphitization process and the formation of a partial nanocrystalline structure of the compound (Mirgorod *et al.* 2016).

As expected, the cassava peel biomass after activation shows a higher development of surface area and pore volume. Indeed, the dehydration process by a chemical activating agent like H_3PO_4 increases the surface area and porosity (Heidarinejad *et al.* 2020). The specific surface area of CPC given by the BET model was found 618.265 m^2/g and the volume of pores is $1.53610^{-1}\,cm^3/g$ with an average pore diameter of 3.016 nm. According to the IUPAC classification (Gaya *et al.* 2015), CPC showed mostly the development of a mesoporous structure. In addition, the shape of the N_2 adsorption–desorption isotherm was type IV (a), showing the presence of well-developed microporosity. Therefore, the adsorption capability of CPC is related to a particular disposition of both micro- and mesoporous texture. N_2 adsorption–desorption isotherm (supplementary figure 10), pore size distribution (supplementary figure 11) and incremental pore volume of CPC (supplementary figure 12) are given in the Supplementary material.

The morphology and structure of the cassava peel carbon CPC were observed by SEM. As shown in Figure 2, the surface area of CPC is predominantly that of an amorphous compound with crystalline components. Moreover, the existence of some particulate matter on the external surface of CPC might be related to the activating agent H_3PO_4.

Table 1 gives the composition on a mass basis of CPR from elemental analysis and the composition, also on a mass basis, of CPC evaluated by EDX, which gives a semi quantitative analysis (just carbon and nitrogen). As noticed, the chemical composition of carbon did not significantly change after the activation step (from 37.7% to 38.65%), while there was a decrease in the oxygen level (from 55.9% to 42.72%. Maybe this is related to the fact that the calcination did not take place in an inert atmosphere. EDX also showed the presence of 14.09% phosphorus. This is due to the use of phosphoric acid as an activating agent, which allows us to predict the acidic surface nature of our adsorbent.

From Figure 3, FTIR analysis of CPR and CPC exhibited a profound transformation during activation, where the disappearance of the absorption band at 1,367 cm^{-1} in the CPC spectrum (present in the CPR spectrum) was noted. This band is attributed to the C-H symmetrical bending of the hemicellulose methoxyl group (Boukir *et al.* 2019). Additionally, the disappearance of the most intense peak in the CPR spectrum at 995 cm^{-1}, associated with the C-O bond of cellulose from C-O-C groups (Ilyas *et al.* 2019), was detected in the CPC spectrum. In the CPC spectrum,

Table 1 | Composition of cassava peel carbon (CPC) and cassava peel raw (CPR)

Adsorbent	C	H	N	O
CPR	37.7	6.1	0.3	55.9
CPC	38.65	–	–	42.72

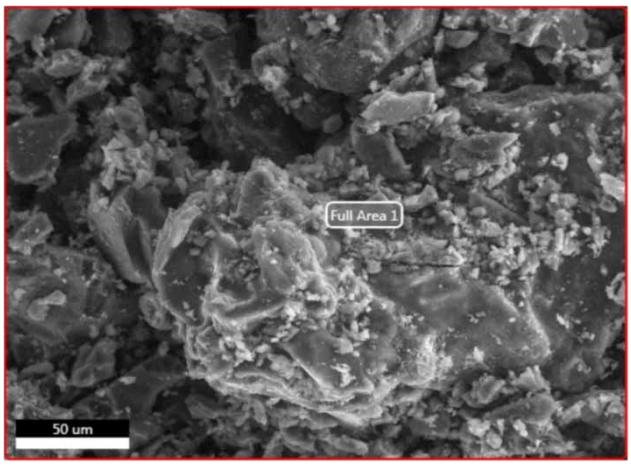

Figure 2 | SEM image of cassava peel carbon.

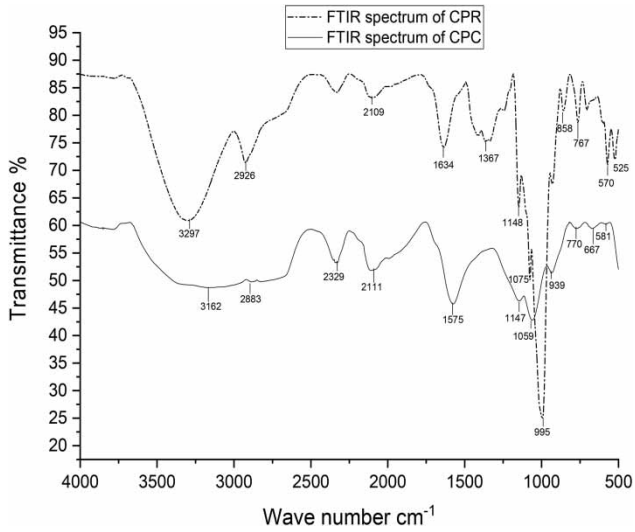

Figure 3 | FTIR spectra of cassava peel carbon (CPC) and cassava peel raw (CPR).

the peaks located at 770 cm^{-1}, 667 cm^{-1} and 581 cm^{-1} corresponded to high crystalline cellulose with the forms I_α and I_β (Lopes *et al.* 2014). Furthermore, the peak at 1,147 cm^{-1} found in both spectra belonged to the aromatic C-H of lignin (Lupoi *et al.* 2015). The peak at 1,575 cm^{-1} is attributed either to the C = C vibration of the aromatic nucleus (Kubovský *et al.* 2020) or to the C = O stretching vibration of the lignin. FTIR results confirmed the disappearance of hemicellulose, crystallization of a part of the cellulose, and better appearance of lignin during the transformation of CPR into CPC. The disappearance of hemicellulose is favoured by the calcination temperature used, and the appearance of crystalline cellulose is in agreement with the XRD analysis. The functional groups of lignin and crystalline cellulose are therefore those involved in the adsorption of heavy metal ions.

Effect of pH

The effect of pH was investigated in preliminary tests. The two metals exhibited better adsorption for pH between 3 and 6. Under those acidic conditions, the CPC surface is protonated by H^+ ions, which favours the electrostatic attraction between $HCr_2O_7^{2-}$ and the positively charged surface while creating a competition between the H^+ ions and Co^{2+} for the adsorption sites. As a result, when the pH increases, the adsorption capacity of chromium and cobalt decreases and increases, respectively (chromium is better adsorbed at pH = 3, while the cobalt adsorption is favoured at pH = 6). However, the adsorption capacities of chromium and cobalt at these optimum pHs are close to the natural pH of each metal solution. For this reason, the kinetic, equilibrium and thermodynamic studies were performed without pH modification.

The variation between final and initial pH was also plotted versus the initial pH to evaluate the pHpzc (Figure 4). The pHpzc is a vital parameter of adsorbents to explore the adsorption mechanisms. The value at which pH final was equal to pH initial was accepted to be pHpzc, and the charge surface is neutral at this pH value; the value of pHpzc was found to be 4.59 for CPC, indicating that the surface of the CPC is negatively charged at pH higher than 4.59 and positively charged at pH lower than 4.59. Moreover, under pHpzc, the adsorption of each metal was favoured.

Effect of initial concentration

The influence of initial concentration on the adsorption of chromium and cobalt is shown in Figure 5; the removal of

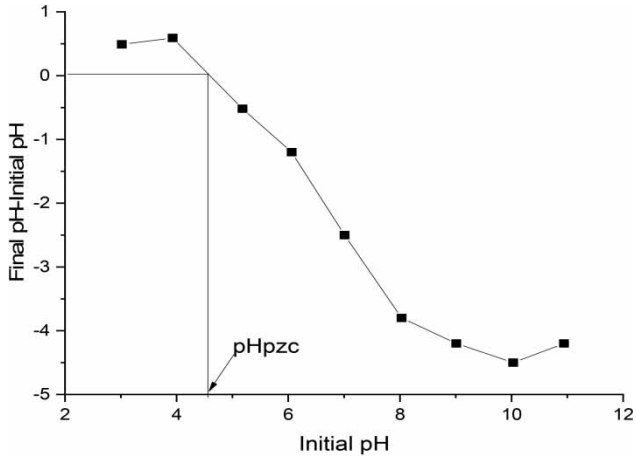

Figure 4 | Determination of point of zero charge of CPC.

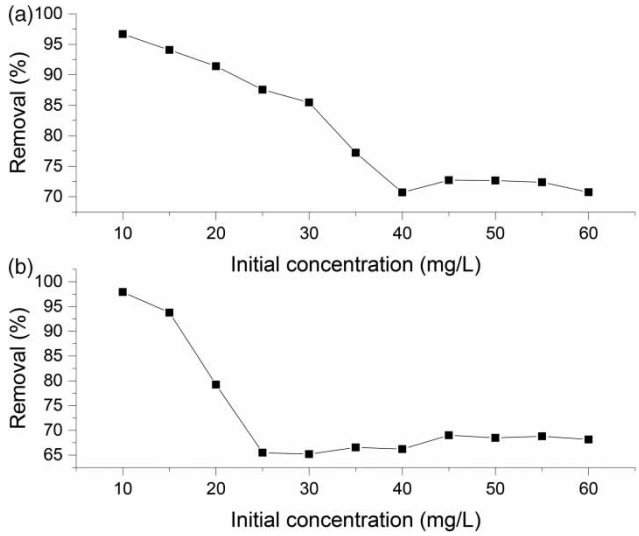

Figure 5 | (a) Effect of initial cobalt concentration on cobalt adsorption and (b) effect of initial chromium concentration on chromium adsorption.

both heavy metal ions decreased with an increase in the initial concentration at a fixed adsorbent dosage (0.02 g) and a temperature of 25°. The reason was that at higher concentrations, the ratio of the initial number of available adsorption sites to cobalt and chromium molecules was low, the number of available adsorption sites became lower, and thus the removal of the two heavy metals was reduced.

Effect of temperature

Figure 6 exhibits the influence of temperature on cobalt and chromium adsorption. It is presented that there is an increase from 234.16 mg/g to 342.5 mg/g in the adsorption

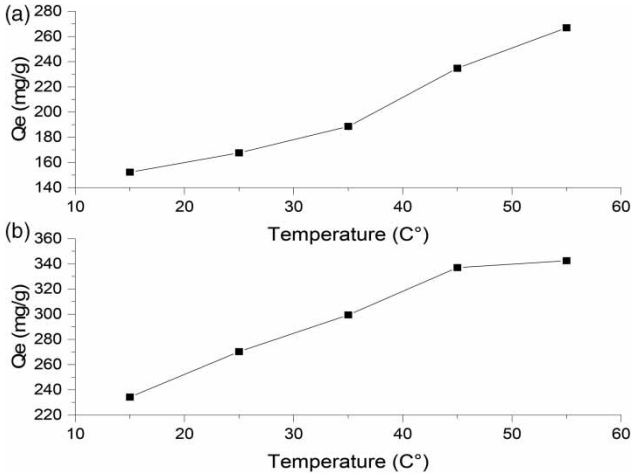

Figure 6 | The effect of temperature on (a) chromium adsorption and (b) cobalt adsorption by cassava peel carbon.

capacity of cobalt as temperature increases from 15 °C to 55 °C, and an increase from 152.20 mg/g to 266.86 mg/g in the adsorption capacity of chromium as temperature increases from 15 °C to 55 °C. The increase of the equilibrium adsorption with increase in temperature indicated that this process was endothermic; this can be explained by the increase in the mobility of cobalt and chromium ions caused by the decrease of the medium's viscosity with increasing temperature of the solution.

Adsorption kinetics

To describe the adsorption kinetic of cobalt and chromium ions on CPC, two models were used, Lagergren's pseudo-first order model and the pseudo-second order model; expressed, respectively, by the following equations:

$$Q_t = Q_e(1 - e^{-k_1 t}) \tag{3}$$

$$Q_t = \frac{k_2 Q_e^2 t}{1 + k_2 Q_e t} \tag{4}$$

where Q_t (mg/g) is the amount of metal ion on the surface of the sorbent at time t (min), Q_e (mg/g) is the amount of metal ion adsorbed at equilibrium. k_1 (min^{-1}) and k_2 (g/mg·min) are the dynamics constants. To determine the goodness of fit of the two kinetic models, the Reduced Chi-Square χ^2 and R-Square R^2 were used as error parameters for each model. The results are shown in Table 2.

The kinetic profiles for the adsorption of the two heavy metal ions are presented separately in Figure 7 and indicate that for both heavy metal ions (chromium and cobalt), the adsorption took place via two stages. The first stage is a fast sorption uptake that occurred within 40 minutes of metal ion and activated carbon contact. The second stage is a slow phase of metal ion removal that developed from 50 min until 180 min when a quasi-stabilised state was presumed to have been reached. The adsorption capacity values at the equilibrium after 180 min were 182.77 mg/g for cobalt ion and 158.47 mg/g for chromium ion. The two-stage kinetic profiles for cobalt and chromium ions can be associated with the nature of available surface sites for adsorption. When the contact between cassava peel carbon and the heavy metal ion is established at the onset of sorption, there are a good number of available sites for sorption to occur; hence the fast metal ion uptake observed. However, as the uptake proceeds and available sites are occupied, the rate of further adsorption decreases due to

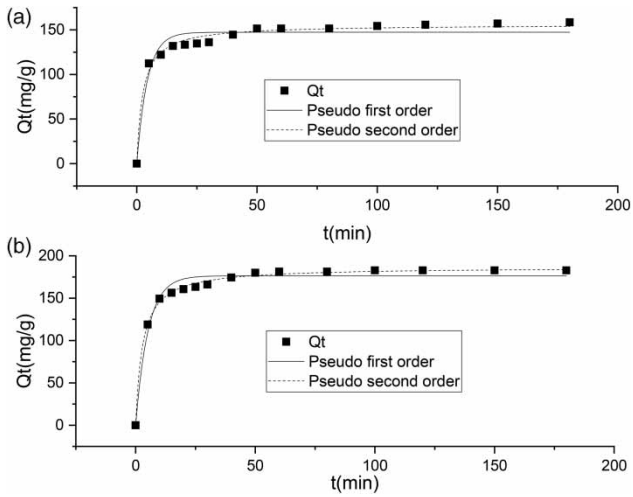

Figure 7 | The pseudo-first order and pseudo-second order equations of (a) chromium and (b) cobalt.

Table 2 | Adsorption kinetic parameters of cobalt and chromium ions on cassava peel carbon (CPC)

		Pseudo-first order model				Pseudo-second order model			
	Qe_{exp} (mg/g)	k_1 (min^{-1})	Reduced Chi square χ^2	Qe_{cal} (mg/g)	R^2	k_2 (g /mg·min)	Reduced Chi square χ^2	Qe_{cal} (mg/g)	R^2
Co(II)	182.77	0.1928	0.62	176.34	0.973	0.00187	0.068	186.75	0.997
Cr(VI)	158.47	0.22805	0.91	147.26	0.945	0.00254	0.21	155.99	0.986

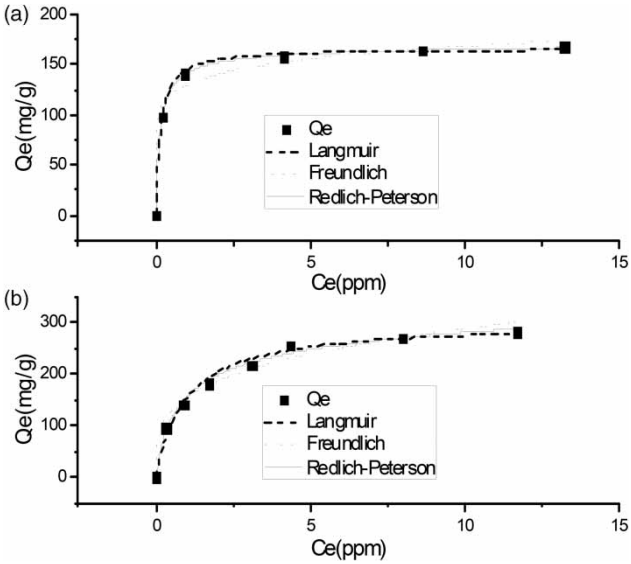

Figure 8 | Langmuir, Freundlich and Redlich-Peterson isotherms plots for sorption of (a) Chromium, (b) cobalt onto cassava peel carbon (CPC).

the repulsive forces between the already adsorbed metal ion and the incoming sorbate and the limitation of available sites for occupation.

Table 2 shows that the pseudo-second order model gives the best fit for the two heavy metal ions, according to: (i) the R^2 coefficient values (0.997 and 0.986 for cobalt and chromium, respectively) higher than the pseudo-first order model (0.973 for cobalt and 0.945 for chromium), (ii) the Reduced Chi-Square (0.068 for cobalt and 0.21 for chromium) lower than the pseudo first order model (0.62 and 0.91 for cobalt and chromium, respectively); similar results was obtained by Scheufele *et al.* (2019), who studied the biosorption of direct black dye by cassava root husks. The value of Reduced Chi-Square (χ^2) of cobalt indicates that the adsorption of this heavy metal onto CPC is best described by the pseudo-second order model. Also, the pseudo-second order constant k_2 for cobalt was 0.00187 g/mg·min, while that for chromium was 0.00254 g/mg·min. This indicates that the sorption of chromium ions onto the CPC was faster than that of cobalt ions; the same result was discussed by Swelam *et al.* (2018), who also investigated the removal of cobalt ions from aqueous solution using raw and modified rice straw. Since the activated carbon has both micropores and mesopores, the adsorption of the ion with the bigger radius (cobalt) may be favoured. Moreover, (iii) the calculated adsorption capacity values at the equilibrium (186.75 mg/g and 155.99 mg/g for cobalt and chromium, respectively) for the pseudo-second order model are closer to the experimental values (182.77 mg/g and 158.47 mg/g for cobalt and chromium, respectively).

Based on these results, the pseudo-second order is the best kinetic model of cobalt and chromium adsorption onto the CPC.

Adsorption isotherms

Adsorption isotherm is the relation between the quantities of substance adsorbed by an adsorbent under equilibrium conditions at constant temperature. Different models were used for determining the adsorption isotherms such as Freundlich, Langmuir and Redlich-Peterson models, given respectively by the following equations:

$$Q_e = K_F C_e^{\frac{1}{n}} \tag{5}$$

$$Q_e = \frac{Q_{max} K_L C_e}{1 + K_L C_e} \tag{6}$$

$$Q_e = \frac{K_R C_e}{1 + \alpha C_e^{\beta}} \tag{7}$$

where Q_{max} (mg/g) is a single-layer maximum adsorption capacity, Q_e (mg/g) is heavy metal adsorption capacity at adsorption equilibrium and C_e (mg/L) is the heavy metal concentration at adsorption equilibrium. The constants are n, K_F, K_L, α, β. When the value of β is equal to 1, the above equation is reduced to the Langmuir isotherm, while when it is equal to 0, the equation is reduced to the Freundlich isotherm.

The Langmuir model can be expressed in terms of a dimensionless constant separation factor R_L (Equilibrium Parameters), which describes the type of isotherm that is given by:

$$R_L = \frac{1}{1 + K_L C_i} \tag{8}$$

where C_i is the initial concentration of the heavy metal. The magnitude of R_L determines the feasibility of the adsorption process.

If $R_L > 1$, adsorption is unfavourable; if $R_L = 1$, adsorption is linear; if $R_L < 1$, adsorption is favourable; and if $R_L = 0$, adsorption is irreversible.

From Table 3, it can be observed that the Freundlich constant K_F, which relates to adsorption capacity, was 129.81 ($mg^{(1-n)}$ L^n/g) for chromium and 153.79 ($mg^{(1-n)}$ L^n/g) for cobalt. This indicates that the loading of cobalt

Table 3 | Adsorption isotherm parameters of cobalt and chromium ions on the cassava peel carbon (CPC)

	Freundlich model				Langmuir model				Redlich-Peterson model				
	K_F (mg$^{(1-n)}$ L^n/g)	n	Chi Square χ^2	R^2	Q_{max} (mg/g)	K_L (L/mg)	Chi Square χ^2	R^2	K_R (L/g)	α (L/mg)	β	Chi Square $\chi 2$	R^2
Cr (VI)	129.81	3.66	0.838	0.98	166.35	6.59	0.054	0.998	1,310.6	8.278	0.97	0.53	0.999
Co (II)	153.79	8.92	0.25	0.977	301.63	1.038	0.21	0.989	468.57	2.015	0.89	0.86	0.993

was higher than that of chromium on the CPC adsorbent. Furthermore, the Freundlich constant n, which relates to the intensity of adsorption, was 3.66 for chromium and 8.92 for cobalt, indicating more favourability of the cobalt ion adsorption on CPC adsorbent. The Langmuir constant K_L, which characterizes the energy constant, was 6.59 (L/mg) for chromium and 1.038 (L/mg) for cobalt, indicating that the chromium adsorbed onto the surface of cassava peel carbon has a lower heat of adsorption. The maximum adsorption capacity Q_{max} for cobalt was 301.63 mg/g and that of chromium was 166.35 mg/g. This indicates that cobalt adsorption was higher on the adsorbent than that of chromium ion. The Redlich-Peterson constant β value was 0.97 for chromium and 0.89 for cobalt, both values tending to 1, so the Redlich-Peterson model reduces to Langmuir model. Furthermore, the R_L value was 0.011 and 0.076 for chromium and cobalt, respectively, indicating that the adsorption is favourable.

To determine the goodness of fit of the Langmuir, Freundlich and Redlich-Peterson isotherm models to the experimental data, non-linear regression and error parameters were used and defined for each model (coefficient of determination (R^2) and the Reduced Chi-Square) (Scheufele *et al.* 2019). The comparison of the fitting parameters of these three models indicates the best model that describes well the isotherm adsorption. Table 3 indicates that the Redlich-Peterson model has high R^2 values for both heavy metals (0.999 for chromium and 0.993 for cobalt) compared with the Langmuir model (0.998 for chromium and 0.989 for cobalt) and the Freundlich model (0.98 for chromium and 0.977 for cobalt). Moreover, the Reduced Chi-Square of the Langmuir model has lower values (0.054 for chromium and 0.21 for cobalt) compared with the Redlich-Peterson model (0.53 for chromium and 0.86 for cobalt) and the Freundlich model (0.838 for chromium and 0.25 for cobalt). Finally, we can conclude that the Redlich-Peterson isotherm is the better, but β values tend to 1, which means that the Langmuir model can explain the adsorption mechanism and the general tendency of the two heavy metal ions is to fill the first layer of the surface of the CPC. We can conclude a monolayer adsorption nature.

In addition, Co (II) adsorption capacity is higher than Cr (VI), while chromium adsorption kinetics is faster. The particular disposition of the microporous and mesoporous pore observed in textural properties may affect the adsorption mechanism. In fact, the difference between the ionic radius of Co (II) (79 ppm) and Cr (VI) (58 ppm) can make the adsorption of chromium faster, as it can fit in micropores (Arshadi *et al.* 2014). But as the activated carbon is mostly mesoporous, the amount of cobalt adsorbed is higher.

From Table 4 we can notice that the mango kernel activated carbon has been found to be less effective as adsorbent material for chromium, with an adsorption capacity of 7.8 mg/g. Date press cake activated carbon has shown the highest adsorption capacity for chromium at 282.8 mg/g. Also in the same table, we can observe that potato peel activated carbon has shown the highest adsorption capacity for

Table 4 | Comparison of adsorption capacity for cobalt and chromium adsorption onto CPC and activated carbons from other raw materials

Adsorbate	Adsorbent	Adsorption capacity (mg/g)	References
Chromium	Banana peel AC	131.56	Memon *et al.* (2009)
	Mango kernel AC	7.8	Rai *et al.* (2016)
	Date press cake AC	282.8	Norouzi *et al.* (2018)
	Cassava peel carbon CPC	166.35	This work
Cobalt	Lemon peel AC	22.00	Bhatnagar *et al.* (2010)
	Rice straw AC	28.5	Swelam *et al.* (2018)
	Hazelnut shells AC	13.88	Demirbas (2003)
	Potato peels AC	405	Kyzas *et al.* (2016)
	Cassava peel carbon CPC	301.63	This work

AC, activated carbon.

cobalt at 405 mg/g compared with other material such as lemon peel activated carbon, rice straw AC, hazelnut shell AC and CPC, which showed only 22.00, 28.5, 13.88 and 301.63 mg/g, respectively.

Thermodynamic study

To get more insights on the nature of the adsorption of cobalt and chromium ions onto CPC, a thermodynamic study was carried out. The thermodynamic parameters enthalpy ΔH_{ads}(kJ/mol), standard entropy ΔS_{ads} kJ/(mol·k), and the Gibbs free energy ΔG_{ads} (kJ/mol) are expressed by the equations bellow:

$$\Delta G_{ads} = -RT\ln(K_d) \quad (9)$$

$$\ln K_d = \frac{\Delta S^\circ}{R} - \frac{\Delta H^\circ}{RT} \quad (10)$$

$$K_d = \frac{Q_e}{C_e}$$

where K_d is the equilibrium constant (L/g), R (8.134 J/(mol·K)) is the gas constant, and T(K) is the absolute temperature. ΔH_{ads} and ΔS_{ads} were obtained from the slope and intercept of the Van't Hoff's plot of $\ln(K_d)$ versus 1/T.

The outcomes are presented in Table 5. The negative value of the Gibbs free energy (ΔG_{ads}) explains the spontaneous nature of the adsorption of cobalt and chromium ions onto CPC; indeed, the adsorption process becomes more spontaneous with rising temperature, which makes the adsorption process more favourable. The endothermic nature of the adsorption process of these two heavy metals is confirmed by the positive values of enthalpy ΔH_{ads}. In addition, generally the enthalpy ΔH_{ads} values less than 40 kJ/mol·K suggest that the adsorption is physical adsorption and reversible. This endothermic character also supports what we explained above regarding the increase in adsorption capacity of CPC with increasing temperature. Furthermore, the standard entropy ΔS_{ads} has positive values and indicates the increase of randomness at the solid-solution interface during adsorption. Finally, as mentioned above, CPC had sufficient surface area, a certain number of surface functional groups, and the largest adsorption capacities for cobalt and chromium. And the adsorption process showed better spontaneity.

Desorption study

The desorption efficiencies for heavy metal ions by using three kinds of desorbing agent (HNO_3, distilled water, NaOH) were in the range of 96.83%–88.28% for cobalt and 96.72%–87.09% for chromium (Figure 9). We can notice also from the figure that desorption in the acidic media (HNO_3) for the two heavy metal ions was more rapid and presented higher cobalt and chromium recovery from the CPC than in basic and neutral media. In acidic medium, the functional groups in the CPC become protonated and do not attract the positively charged metal ions, and so the protons (H^+) replace the bound metal ions. Therefore, the metal ions cannot compete with H^+ ions for adsorption sites, and subsequently metal ions are released from the adsorbent surface into the solution.

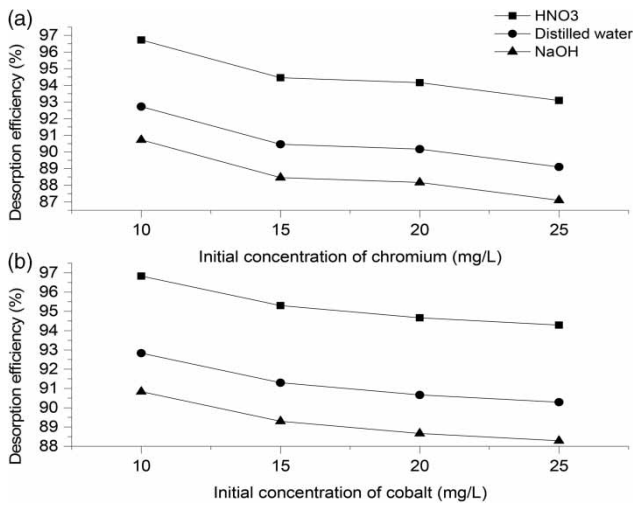

Figure 9 | Effect of desorbing agent on the recovery of (a) chromium, (b) cobalt from cassava peel carbon.

Table 5 | Thermodynamic parameters of the adsorption of cobalt and chromium ions on the cassava peel carbon (CPC)

Parameters	ΔH_{ads}	ΔS_{ads}	ΔG_{ads}			Q_e		
Units	kJ/mol	kJ/mol·k	kJ/mol			mg/g		
Temperatures	–	–	15	25	35	15	25	35
Chromium	18.28	0.063	− 5.58	− 6.29	− 7.24	152.21	167.58	188.56
Cobalt	39.64	0.16	− 7.20	− 8.73	− 10.45	234.16	270.20	299.44

CONCLUSION

In conclusion, cassava peel carbon (CPC) has shown its potential to be an effective agricultural waste material valorized for heavy metal removal from aqueous solution. It is found that the kinetic adsorption data of cobalt and chromium was well fitted to the pseudo-second order model, while the adsorption isotherms were fitted to the Langmuir isotherm model, which confirm the monolayer adsorption nature of cobalt ions and chromium ions on CPC. Likewise, the thermodynamic study showed that the adsorption process on the CPC is endothermic, spontaneous and follows a physisorption process. Differences between Cr (VI) and Co (II) adsorption performances may be attributed to the pH effect. Electrostatic attraction/repulsion explains the fact that cobalt adsorption capacity was higher than chromium.

DATA AVAILABILITY STATEMENT

All relevant data are included in the paper or its Supplementary Information.

REFERENCES

Akpomie, K. G. & Dawodu, F. A. 2014 Treatment of an automobile effluent from heavy metals contamination by an eco-friendly montmorillonite. *Journal of Advanced Research* **6** (6), 1003–1013. http://dx.doi.org/10.1016/j.jare.2014.12.004.

Arshadi, M., Amiri, M. J. & Mousavi, S. 2014 Kinetic, equilibrium and thermodynamic investigations of Ni(II), Cd(II), Cu(II) and Co(II) adsorption on barley straw ash. *Water Resources and Industry* **6**, 1–17. http://dx.doi.org/10.1016/j.wri.2014.06.001.

Beakou, B. H., El Hassani, K., Houssaini, M. A., Belbahloul, M., Oukani, E. & Anouar, A. 2017 A novel biochar from *Manihot esculenta* Crantz waste: application for the removal of Malachite Green from wastewater and optimization of the adsorption process. *Water Science and Technology* **76** (6), 1447–1456. https://doi.org/10.2166/wst.2017.332.

Bhatnagar, A., Minocha, A. K. & Sillanpää, M. 2010 Adsorptive removal of cobalt from aqueous solution by utilizing lemon peel as biosorbent. *Biochemical Engineering Journal* **48** (2), 181–186.

Boukir, A., Fellak, S. & Doumenq, P. 2019 Structural characterization of *Argania spinosa* Moroccan wooden artifacts during natural degradation progress using infrared spectroscopy (ATR-FTIR) and X-Ray diffraction (XRD). *Heliyon* **5** (9), e02477. https://doi.org/10.1016/j.heliyon.2019.e02477.

Demirbas, E. 2003 Adsorption of cobalt (II) ions from aqueous solution onto activated carbon prepared from Hazelnut Shells. *Adsorption Science & Technology* **21** (10), 951–963. https://doi.org/10.1260/02636170360744380.

Farjana, S. H., Huda, N. & Mahmud, M. A. P. 2019 Life cycle assessment of cobalt extraction process. *Journal of Sustainable Mining* **18** (3), 150–161. https://doi.org/10.1016/j.jsm.2019.03.002.

Gaya, U. I., Otene, E. & Abdullah, A. H. 2015 Adsorption of aqueous Cd(II) and Pb(II) on activated carbon nanopores prepared by chemical activation of doum palm shell. *SpringerPlus* **4** (1), 458. https://doi.org/10.1186/s40064-015-1256-4.

Hashemian, S., Salari, K. & Yazdi, Z. A. 2014 Preparation of activated carbon from agricultural wastes (almond shell and orange peel) for adsorption of 2-pic from aqueous solution. *Journal of Industrial and Engineering Chemistry* **20** (4), 1892–1900. http://dx.doi.org/10.1016/j.jiec.2013.09.009.

Heidarinejad, Z., Dehghani, M. H., Heidari, M., Javedan, G., Ali, I. & Sillanpää, M. 2020 Methods for preparation and activation of activated carbon: a review. *Environmental Chemistry Letters* **18** (2), 393–415. https://doi.org/10.1007/s10311-019-00955-0.

Ilyas, R. A., Sapuan, S. M., Ibrahim, R., Abral, H., Ishak, M. R., Zainudin, E. S., Atikah, M. S. N., Mohd Nurazzi, N., Atiqah, A., Ansari, M. N. M., Syafri, E., Asrofi, M., Sari, N. H. & Jumaidin, R. 2019 Effect of sugar palm nanofibrillated cellulose concentrations on morphological, mechanical and physical properties of biodegradable films based on agro-waste sugar palm (*Arenga pinnata*(Wurmb.) Merr) starch. *Journal of Materials Research and Technology* **8** (5), 4819–4830. https://doi.org/10.1016/j.jmrt.2019.08.028.

Javanbakht, V., Alavi, S. A. & Zilouei, H. 2014 Mechanisms of heavy metal removal using microorganisms as biosorbent. *Water Science and Technology* **69** (9), 1775–1787. https://doi.org/10.2166/wst.2013.718.

Kubovský, I., Kačíková, D. & Kačík, F. 2020 Structural changes of oak wood main components caused by thermal modification. *Polymers* **12** (2), 485. https://doi.org/10.3390/polym12020485.

Kyzas, G. Z., Deliyanni, E. A. & Matis, K. A. 2016 Activated carbons produced by pyrolysis of waste potato peels: Cobalt ions removal by adsorption. *Colloids and Surfaces A: Physicochemical and Engineering Aspects* **490**, 74–83. http://dx.doi.org/10.1016/j.colsurfa.2015.11.038.

Lopes, T. D., Riegel-Vidotti, I. C., Grein, A., Tischer, C. A. & Faria-Tischer, P. C. d. S. 2014 Bacterial cellulose and hyaluronic acid hybrid membranes: production and characterization. *International Journal of Biological Macromolecules* **67**, 401–408. http://dx.doi.org/10.1016/j.ijbiomac.2014.03.047.

Lupoi, J. S., Singh, S., Parthasarathi, R., Simmons, B. A. & Henry, R. J. 2015 Recent innovations in analytical methods for the qualitative and quantitative assessment of lignin. *Renewable and Sustainable Energy Reviews* **49**, 871–906. http://dx.doi.org/10.1016/j.rser.2015.04.091.

Memon, J. R., Memon, S. Q., Bhanger, M. I., El-Turki, A., Hallam, K. R. & Allen, G. C. 2009 Banana peel: a green and

economical sorbent for the selective removal of Cr(VI) from industrial wastewater. *Colloids and Surfaces B: Biointerfaces* **70** (2), 232–237.

Mirgorod, Y., Emelianov, S., Fedosjuk, V. & Bolshanina, S. 2016 Influence of size effects on the properties of processed iron ore and schungite rock. *Journal of Nano- and Electronic Physics* **8** (2), 0–6. https://doi.org/10.21272/jnep.8(2).02053.

Norouzi, S., Heidari, M., Alipour, V., Rahmanian, O., Fazlzadeh, M., Mohammadi-moghadam, F., Nourmoradi, H., Goudarzi, B. & Dindarloo, K. 2018 Preparation, characterization and Cr(VI) adsorption evaluation of NaOH-activated carbon produced from date press cake; an agro-industrial waste. *Bioresource Technology* **258** (Vi), 48–56. https://doi.org/10.1016/j.biortech.2018.02.106.

Pugazhenthiran, N., Anandan, S. & Ashokkumar, M. 2016 Removal of heavy metal from wastewater. *Handbook of Ultrasonics and Sonochemistry* (January), 813–839. https://doi.org/10.1007/978-981-287-278-4_58.

Rai, M. K., Shahi, G., Meena, V., Meena, R., Chakraborty, S., Singh, R. S. & Rai, B. N. 2016 Removal of hexavalent chromium Cr (VI) using activated carbon prepared from mango kernel activated with H_3PO_4. *Resource-Efficient Technologies* **2**, S63–S70. http://dx.doi.org/10.1016/j.reffit.2016.11.011.

Rai, P. K., Lee, S. S., Zhang, M., Tsang, Y. F. & Kim, K. H. 2019 Heavy metals in food crops: health risks, fate, mechanisms, and management. *Environment International* **125** (January), 365–385. https://doi.org/10.1016/j.envint.2019.01.067.

Rangabhashiyam, S., Nandagopal, M. S. G., Nakkeeran, E. & Selvaraju, N. 2016 Adsorption of hexavalent chromium from synthetic and electroplating effluent on chemically modified *Swietenia mahagoni* shell in a packed bed column. *Environmental Monitoring and Assessment* **188** (7), 411. http://dx.doi.org/10.1007/s10661-016-5415-z.

Saha, S., Zubair, M., Khosa, M. A., Song, S. & Ullah, A. 2019 Keratin and chitosan biosorbents for wastewater treatment: a review. *Journal of Polymers and the Environment* **27** (7), 1389–1403. https://doi.org/10.1007/s10924-019-01439-6.

Salgaonkar, B. B., Mani, K. & Bragança, J. M. 2019 Sustainable bioconversion of cassava waste to poly(3-hydroxybutyrate-co-3-hydroxyvalerate) by *Halogeometricum borinquense* Strain E3. *Journal of Polymers and the Environment* **27** (2), 299–308. http://dx.doi.org/10.1007/s10924-018-1346-9.

Scheufele, F. B., Ueda, M. H., Ribeiro, C., Steffen, V., Borba, C. E. & Kroumov, A. D. 2019 Biosorption of direct black dye by cassava root husks: kinetics, equilibrium, thermodynamics and mechanism assessment. *Environmental Chemical Engineering* **8** (2), 103533. https://doi.org/10.1016/j.jece.2019.103533.

Swelam, A. A., Awad, M. B., Salem, A. M. A. & El-Feky, A. S. 2018 An economically viable method for the removal of cobalt ions from aqueous solution using raw and modified rice straw. *HBRC Journal* **14** (3), 255–262. http://dx.doi.org/10.1016/j.hbrcj.2016.10.001.

Tejada-Tovar, C., Gonzalez-Delgado, A. D. & Villabona-Ortiz, A. 2019 Characterization of residual biomasses and its application for the removal of lead ions from aqueous solution. *Applied Sciences (Switzerland)* **9** (21), 4486. http://dx.doi.org/10.3390/app9214486.

World Health Organization 2003 *Chromium in Drinking-Water. Background Document for Preparation of WHO Guidelines for Drinking-Water Quality*. World Health Organization, (WHO/SDE/WSH/03.04/4), Geneva.

World Health Organization. Office of Occupational Health 1996 *Biological Monitoring of Chemical Exposure in the Workplace: Guidelines*. Available from: http://apps.who.int/iris/bitstream/10665/41856/1/WHO_HPR_OCH_96.1.pdf.

Zbair, M., Ainassaari, K., Drif, A., Ojala, S., Bottlinger, M., Pirilä, M., Keiski, R. L., Bensitel, M. & Brahmi, R. 2018 Toward new benchmark adsorbents: preparation and characterization of activated carbon from argan nut shell for bisphenol A removal. *Environmental Science and Pollution Research* **25** (2), 1869–1882. http://dx.doi.org/10.1007/s11356-017-0634-6.

First received 25 June 2020; accepted in revised form 23 November 2020. Available online 8 December 2020